Pore formation in 1,2-dimyristoyl-sn-glycero-3-phosphocholine/cholesterol mixed bilayers by low concentrations of antimicrobial peptide melittin

ARTICLE *in* COLLOIDS AND SURFACES B: BIOINTERFACES · SEPTEMBER 2014

Impact Factor: 4.15 · DOI: 10.1016/j.colsurfb.2014.09.037 · Source: PubMed

4 AUTHORS, INCLUDING:

Lu Zhou
Chinese Academy of Sciences
11 PUBLICATIONS **10** CITATIONS
SEE PROFILE

Ganesan Narsimhan
Purdue University
92 PUBLICATIONS **1,765** CITATIONS
SEE PROFILE

Colloids and Surfaces B: Biointerfaces 123 (2014) 419–428

Contents lists available at ScienceDirect

Colloids and Surfaces B: Biointerfaces

journal homepage: www.elsevier.com/locate/colsurfb

Pore formation in 1,2-dimyristoyl-sn-glycero-3-phosphocholine/cholesterol mixed bilayers by low concentrations of antimicrobial peptide melittin

Lu Zhou [b,1], Ganesan Narsimhan [a,*,1], Xiayou Wu [a], Fengpei Du [b]

[a] Department of Agricultural and Biological Engineering, Purdue University, West Lafayette, IN 47907, USA
[b] Department of Applied Chemistry, College of science, China Agriculture University, 2 Yuanmingyuan Xilu, Haidian Dist., Beijing 100193, China

ARTICLE INFO

Article history:
Received 19 June 2014
Received in revised form 8 September 2014
Accepted 16 September 2014
Available online 28 September 2014

Keywords:
Antimicrobial peptide
Pore formation
Lipid bilayer
DMPC
Cholesterol
Melittin
Lag time

ABSTRACT

Antimicrobial peptides (AMP) represent a class of compounds to combat antibiotic resistance to microorganisms, neutralize biological warfare agents, and as topical antimicrobial agents. AMP kills microbial cells through insertion and permeabilization of the cytoplasmic membranes. It is important to predict the efficacy of AMP at low concentration to circumvent their toxicity. Leakage of fluorescent dyes (calcein, FD4 and FD20) of different molecular weights entrapped within 1,2-dimyristoyl-sn-glycero-3-phosphocholine (DMPC)/cholesterol mixed liposomes by AMP melittin indicated (i) a critical melittin concentration for pore formation and (ii) a lag time for pore formation above this critical concentration. The lag time decreased with an increase in melittin concentration and was in the order FD20 > FD4 > calcein. % α helix of melittin increased when exposed to liposome with this increase being more pronounced at higher concentrations eventually reaching an asymptotic value. The rate of dye leakage following the lag time was found to be larger at higher melittin concentration. A simplified mathematical model for nucleation and growth of pores formed by an aggregate of melittin in lipid bilayer is proposed to predict the variation of rate of dye leakage with melittin concentration which agreed fairly well with the data for calcein and seems to suggest a toroidal mechanism of pore formation with participation of large number of phospholipid heads.

1. Introduction

Antimicrobial peptides (AMP) have the ability to penetrate cell membrane and kill the cell either by cell membrane rupture or through disruption of cell function. They are divided into subgroups on the basis of their amino acid composition and structure [1]. Pore formation by AMP in phospholipid bilayers begins by electrostatic attraction followed by attachment and penetration of the cell membrane and has been subject of several investigations [2–6]. Experimental techniques based on fluorescence [7], oriented circular dichroism [4], NMR spectroscopy [8], X-ray crystallography [4] and quartz crystal microbalance [9] have been employed to monitor the pore formation, secondary conformation of AMP, orientation of AMP and the lipid, thinning of the membrane and mass as well as rigidity of the membrane. Peptides have been shown to bind in two physically distinct states [10]. At low peptide/lipid ratios, α-helical peptides, β-sheet peptides and θ-defensins adsorb and embed into the lipid head group region in a functionally inactive state that stretches the membrane [11,12]. At high peptide/lipid ratios, peptide molecules are orientated perpendicularly and insert into the bilayer [4]. Several studies of pore formation by AMP on model membranes has elucidated different mechanisms of pore formation such as *barrel stave*, *toroidal* or *carpet mechanism* and has helped to identify key factors that control pore formation [3,6,8,12–15].

Since the mechanism of deactivation of microorganisms by AMPs differs from that of antibiotics, they could be very useful for combating drug resistant microbes, for treatment of microbial infections and also for prevention. It is customary to report the effectiveness of AMP as minimum inhibitory concentration. In order to circumvent the problem of toxicity, however, very low doses of these AMPs have to be effective in antimicrobial action. With this in mind, we investigated pore formation at very low concentrations through leakage of fluorescent dyes from liposomes and discovered the existence of a time lag for pore formation by AMP above this critical concentration. Consequently, the effectiveness of AMP at very low concentrations can be quantified by this critical concentration and the time lag at higher concentrations.

* Corresponding author. Tel.: +1 765 494 1199; fax: +1 765 496 1115.
E-mail address: narsimha@purdue.edu (G. Narsimhan).
[1] These authors contributed equally to this work.

http://dx.doi.org/10.1016/j.colsurfb.2014.09.037
0927-7765/

Nomenclature

$g_{formation}(n_a, n_b)$	free energy of formation of pore consisting of n_a peptides and n_b phospholipids per peptide
$d_{pore}(n_a, n_b)$	diameter of pore consisting of n_a peptides and n_b phospholipids per peptide
λ	line tension of hydrophilic head of lipid molecule
γ	interfacial tension of phospholipid bilayer
d_h	diameter of phospholipid head
κ	Debye Huckel parameter
l	length of lipid tail
k	Boltzmann constant
T	temperature
ξ	flexibility parameter of peptide molecule
q	net charge of peptide molecule
ϕ	electrostatic potential
σ^*	surface charge density
t_{pore}	thickness of the bilayer
ε_r	dielectric constant of aqueous medium inside the pore
ε_0	permittivity of vacuum
q_{ph}	net charge of phospholipid head
g_{bend}	bending free energy of phospholipid heads
$\Delta G_{pep,ads}$	free energy of adsorption of peptide onto phospholipid membrane
$\Delta G_{pore}(n_a, n_b)$	free energy of pore consisting of n_a peptides and n_b phospholipids per peptide with respect to adsorbed peptides
$\Delta G_{sol}(n_a, n_b)$	free energy of pore consisting of n_a peptides and n_b phospholipids per peptide with respect to peptides in solution
X	binding constant of peptide onto phospholipids
σ_s	surface free energy change per unit length for pore formation
s	supersaturation
c_p	bulk peptide concentration
c_{ps}	critical peptide concentration for pore formation
n_c	number of peptides in a pore of critical size
ΔG^*	free energy of pore of critical pore size
J	rate of nucleation of pores per unit volume
ρ_{eq} (1)	surface concentration of adsorbed peptides on phospholipid surface
ρ_{eq} (n_c)	surface concentration of pores of critical size
$\dot{n}$	rate of growth of pores
t_g	time of growth of pores
$N(n, t)$	number of pores of size n at time t
c_b	bulk concentration of fluorescent dye
ϕ	volume fraction of liposomes
d_{lip}	liposome diameter
D	diffusion coefficient of dye through pores
D_s	surface diffusion coefficient of peptides on liposome surface
F	fluorescence intensity of dye
$F_{\max}$	maximum fluorescent intensity of dye
t_{lag}	time lag for fluorescence

2. Materials and methods

2.1. Materials

DMPC and cholesterol were obtained from Avanti Polar Lipids, Inc. (Alabaster, AL), dihexadecyl hydrogen phosphate, calcein, fluorescein isothiocyanate-labeled dextrans with average molecular masses of 4 and 20 kDa (FD4 and FD20) and melittin (purity: 91.8%, HPLC) from honey bee venom were purchased from Sigma–Aldrich (St. Louis, MO). Sephadex G-75 (GE Healthcare) was used to separate free calcein from liposomes. The composition of the bilayer is chosen to mimick the cell membrane.

2.2. Preparation of liposomes

Liposome of composition DMPC, cholesterol, and dihexadecyl hydrogen phosphate in a molar ratio of 5:4:1 and with entrapped dye (calcein, FD4 or FD20) was prepared using protocol described elsewhere [16–19]. 100 μl of lipid stock solution (DMPC, cholesterol, and dihexadecyl hydrogen phosphate in a molar ratio of 5:4:1 [16] in chloroform) was dried under N_2 to form a thin film in a glass vial. Three fluorescent reporter molecules, calcein [17], FD4 (molecular weight 4000) and FD20 (molecular weight 20,000) [18] were trapped inside the lumen of the liposomes. Dye entrapment was accomplished by adding 1 ml of calcein (50 mM), FD4 or FD20 (10 mg/ml) in 0.02 M phosphate buffer at pH 6.0 to the lipid film before liposome formation. The suspension was vortexed for several minutes and then allowed to rest for 30 min to form large unilamellar, dye-encapsulating vesicles. The vesicle suspension was then forced through a 1000 nm polycarbonate filter (Avanti Polar Lipids) for clacein, FD4 and FD20 using a miniextruder (Avanti Polar Lipids, Inc.) with two gastight Hamilton syringes [16] fifteen times to form unilamellar liposomes. The diameter of the liposomes was measured by laser light scattering (Zetasizer nano series, Malvern Instruments, Worcestershire, UK). Free dye was removed by size-exclusion chromatography using a Sephadex G-75 column for calcein[19], FD4 and FD20. To avoid photobleaching, both liposomes were stored in a dark environment at −4 °C until use.

2.3. Fluoroscence measurement

The fluorescence of the released dye was measured with a spectrofluorometer (Flex Station II, Molecular Device) at an excitation wavelength of 488 nm and an emission wavelength of 518.5 nm. All experiments were conducted at 25 °C which is above the phase transition temperature for DMPC–cholesterol mixtures of cholesterol concentration above 12.5 mol% [20].

2.4. Circular dichroism (CD)

CD spectra were recorded at room temperature using a Jasco 810 spectropolarimeter (Jasco Spectroscopic Co., Hachioji, Japan) with a quartz cell of 0.2 cm path-length. Data were collected every 0.2 nm with 2 nm bandwidth, at a scan speed of 100 nm/min. Molar ellipiticity (deg cm^{-1} $dmol^{-1}$) is expressed on a mean residue concentration basis in the far-UV. Spectra were analyzed for secondary structure content by using the program *Contin* [21].

2.5. Confocal laser-scanning microscopy (CLSM)

CLSM images were taken using LSM710 (Carl Zeiss, Göttingen, Germany) with an argon ion laser (488 nm). Liposome with encapsulated calcein was mixed with different concentration of melittin. The poly-L-lysine slide was used to fix the sample. The fluorescence intensity was measured as a function of time. Images were then recorded digitally in a 512 × 512 pixel format.

3. Results

The liposomes were monodispersed with a narrow distribution around the mean size of 551 nm. The liposome concentration in the collected fraction from size exclusion chromatographic column is inferred from the measurement of count rate that is obtained from

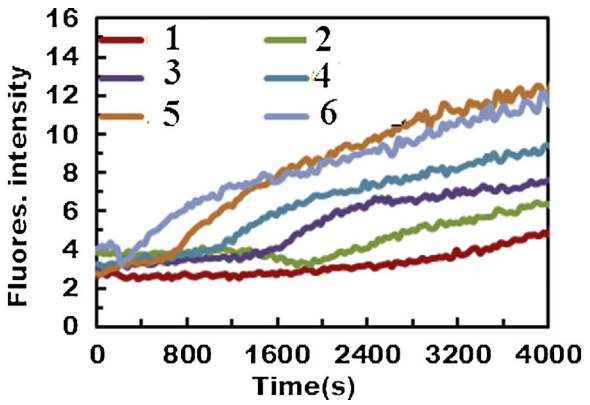

Fig. 1. Fluorescence intensity vs time for different surface concentration of melittin (expressed as *Q*, # of melittin molecules/# of lipid molecules) for leakage of entrapped FD4. The values of *Q* for different curves are: curve 1 – 0.1027; curve 2 – 0.1466; curve 3 – 0.171; curve 4 – 0.2042; curve 5 – 0.2566; curve 6 – 0.5131.

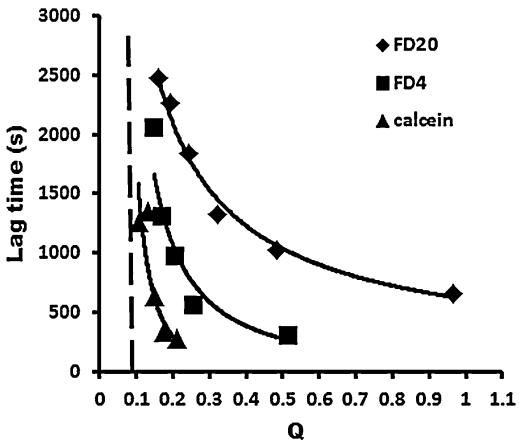

Fig. 2. Lag time for fluorescent dye leakage vs melittin to lipid ratio *Q* (expressed as # of melittin molecules/# of lipid molecules) for the three dyes calcein, FD4 and FD20.

zetameter by referring to the calibration curve that is shown in Fig. S1 (supplemental information). The calibration curve between the count rate and lipid concentration was obtained from standard samples of known concentrations of liposome without any dye. Flourescence intensity of dye FD4 leaked from liposome at different times when exposed to different melittin concentration (different melittin lipid ratio *Q*, expressed as # of melittin molecules per lipid molecule) is shown in Fig. 1. Similar plots of fluorescence vs time for leakage of calcein and FD20 dyes are given in Figs. S2 and S3 (supplemental information) respectively. The fluorescence intensity increases with time and plateaus to a constant value at sufficiently long times. The fluorescence intensity is found to be lower for lower melittin/liposome ratio *Q*. For example, the fluorescence intensity reaches a value of around 12 for melittin/lipid ratio of 0.513 whereas the intensity is about 5 for melittin/lipid ratio of 0.1027. In addition, there is a distinct lag time for this increase especially at lower melittin/lipid ratios (lower melittin concentrations). The lag time is determined from the intersection of the fitted curves of flourescence intensity vs time for the initial phase (when intensity is more or less constant) and for times at which the intensity just starts to increase (see supplemental Fig. S4). The lag time is found to increase dramatically at lower melittin concentration (lower melittin/lipid ratio) and asymptotically reach infinite value at a critical melittin/liposome ratio as can be seen from Fig. 2. Interestingly, the values of this critical melittin/lipid ratio (asymptote) are found to be close to 0.1 for all three dyes, namely, calcein, FD4 and FD20 in spite of the differences in their size (molecular weight). However, the lag time is found to be larger for higher molecular weight dye (FD20 > FD4 > calcein). CD spectra of melittin in the presence of liposome for low and high melittin/liposome ratios are shown in Fig. S5a. There is a shift in CD spectrum (see Fig. S5a), this shift being dependent on melittin/lipid ratio. The CD spectrum was analyzed using *contin* to obtain the relative proportions of α helix, β sheet and random coil. The results (not shown) indicate that there is a decrease in random coil with a corresponding change in other conformations at higher melittin/lipid ratio. This is also evident from the plots of evolution of % α helix for different melittin/lipid ratio as shown in Fig. S5b. The % α helix increases with time and exhibits a maximum value. It is to be noted that the CD spectrum that is obtained is from the melittin in aqueous phase as well as from adsorbed at the liposome interface. In case of higher melittin/lipid ratio (higher melittin concentration), larger fraction of melittin is at the interface, as evidenced by melittin binding isotherm reported by Kuchinka and Seelig [22] thereby resulting in a larger shift in the measured CD spectrum compared to the reference (melittin in aqueous phase).

As described in Section 2, confocal images of very large liposomes containing calcein were captured at different times in order to monitor dye leakage. Since the images are visible for dye of sufficiently high concentrations, these images depict only calcein that is trapped inside the liposome. The sequence of images in Fig. 3a

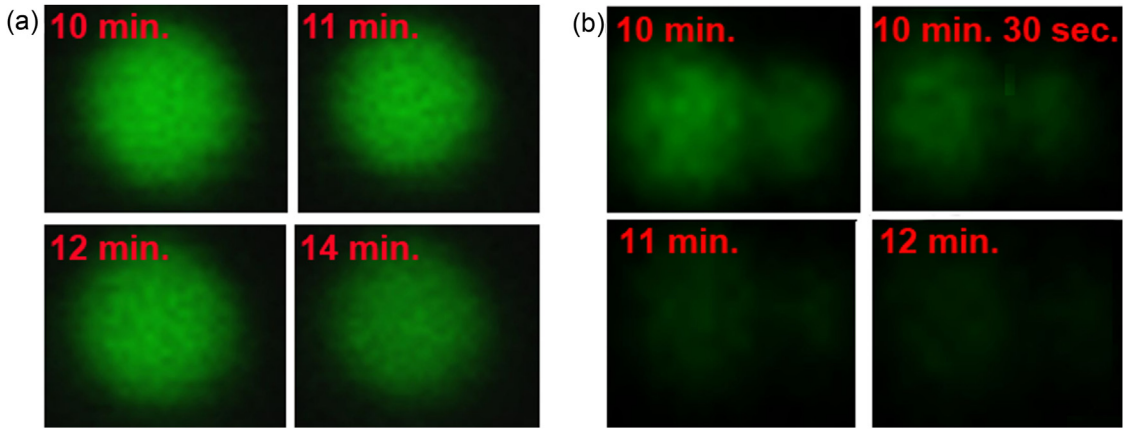

Fig. 3. Fluorescence confocal image for liposome at different times. (a) Liposome with entrapped calcein only; (b) liposome with entrapped calcein treated with 0.7 μM melittin. The indicated time refers to the time elapsed since 10 min after the preparation of the samples.

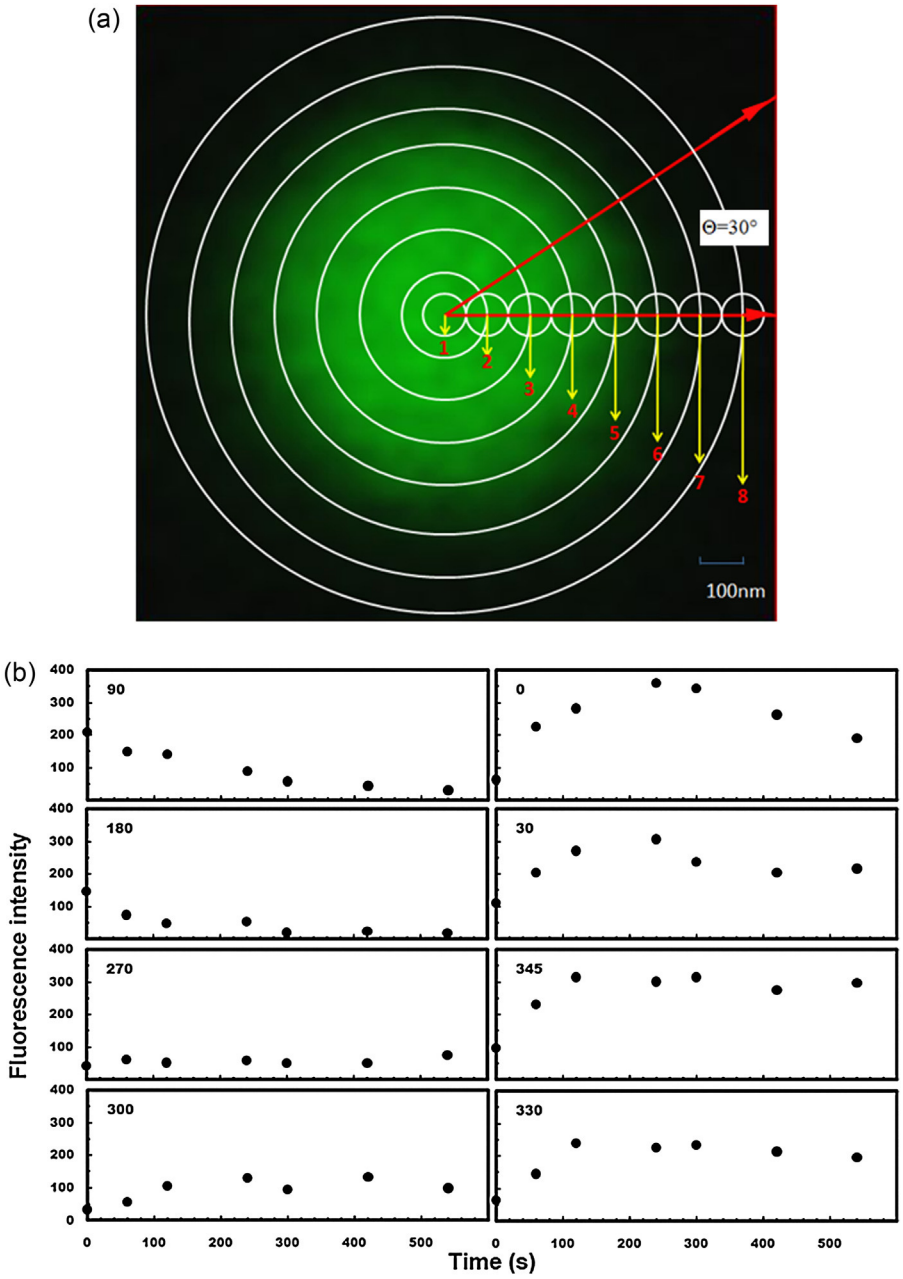

Fig. 4. (a) Typical fluorescence confocal image of one liposome with entrapped fluorescence dye calcein. Eight different concentric regions of 100 nm thickness are indicated in the figure. Also indicated in the figure are two planes corresponding to $\theta = 0$ and $\theta = 30$. (b) Fluorescence intensity vs time for 6th region of confocal image of liposome when exposed to 0.7 μM melittin.

and b show the evolution of dye concentration inside the liposome in the absence and in the presence of 0.7 μM melittin. Dye intensity decays much more rapidly in the presence of melittin (Fig. 3b). Liposome disintegrates in the presence of melittin whereas it was found to be intact when not exposed to melittin. The fluorescence intensity in different regions of cross sectional planes corresponding to different angles between 0° to 360° in 30° increments were monitored with time (two cross sections corresponding to the angles 0° and 30° are shown in Fig. 4a). The fluorescence intensity vs time at different angles for high melittin concentrations for region 6 are shown in Fig. 4b. Similar plots for liposome when exposed to high concentration of melittin for regions 2 and 8 are shown in Figs. S6 and S7 respectively. The fluorescence intensity data for other regions are not shown. The following conclusions can be made from these images, (i) close to center (regions 1 and 2), intensity decreases due to leakage of dye; (ii) in the immediate vicinity of liposome (regions 6, 7 and 8), intensity increases because of accumulation of leaked dye and (iii) the effect of dye leakage is observed only in some angles and not in others. This may indicate pore formation only in some regions within the liposome.

4. Discussion

Pore formation occurs by insertion of an aggregate of melittin of α helical conformation perpendicular to the lipid bilayer which involves adsorption of melittin followed by its aggregation and penetration into bilayer. In other words, melittin is first adsorbed onto the lipid surface by diffusion which is followed by formation of

its surface aggregates by surface diffusion. These aggregates will then penetrate the bilayer by orienting themselves perpendicular to the bilayer. Oriented CD measurements [4,11,23] show that the peptides orient predominantly perpendicular to the lipid membrane above a critical peptide to lipid ratio whereas neutron scattering measurements for melittin [12] and alamecithin [24,25] indicate formation of transmembrane pores only for perpendicular orientation. Consequently, a minimum surface concentration of melittin on lipid bilayer surface is necessary to initiate pore formation. Penetration of surface aggregate will lead to formation of a pore with aqueous inner core. Melittin aggregate is believed to form *toroidal* pore in which the inserted polypeptides induce the lipid molecules to bend so as to line the interior with hydrophilic heads [6,12,13]. The pore is therefore lined by both the hydrophilic part of the peptide aggregate as well as interspersed phospholipid head. Consequently, the peptide charge is partly neutralized by the charge of phospholipid head so as to reduce the unfavorable columbic interactions within the pore. There is an increase in free energy of hydrophilic heads that are pulled apart to form the pore as a result of their line tension. There is also an increase in the free energy as a result of bending of hydrophilic phospholipid head of bilayer. The net effect of these interactions will be an energy barrier which has to be overcome by the aggregate to penetrate the bilayer. The rate of pore formation will be dictated by this energy barrier. Since the rate of adsorption of AMP from bulk to the lipid bilayer surface is proportional to bulk concentration, the time it takes for the surface concentration of AMP to reach this critical value for pore formation is larger at lower concentrations which manifests as lag time for dye leakage. Therefore, dye leakage can be considered to occur in two stages, namely, initiation of pore formation followed by increase in number of pores as well as growth of pores. Both events in the second stage will lead to leakage of fluorescent dye.

Experimental data indicate that there is a critical peptide concentration, below which dye leakage is not observed, i.e. pore formation does not occur. This critical peptide concentration can be considered to be analogous to solubility. This is also consistent with observations that peptides tend to orient perpendicular to the lipid bilayer upon adsorption only about a critical concentration since pore formation by peptide penetration of the bilayer is more likely in vertical orientation [12]. At peptide concentrations above these critical peptide concentrations, pore formation occurs as evidenced by dye leakage with a lag time. Pore formation occurs by an aggregate of peptides in α helical conformation that line the pores with the hydrophobic functional groups pointing outwards toward the lipid tails. The inside of the pore is aqueous.

4.1. Free energy of formation

The free energy of formation of pore $g_{formation}$ is given by

$$g_{formation}(n_a, n_b) = \lambda\pi d_{pore}(n_a, n_b) - \gamma\frac{\pi}{4}d_{pore}(n_a, n_b)^2 \quad (1)$$

where λ is the line tension of hydrophilic head of lipid molecule and γ is the interfacial tension of phospholipid bilayer, n_a and n_b are the number of peptides and number of bent phospholipid heads per peptide in the pore respectively and $d_{pore}(n_a, n_b)$ is the pore diameter. In the above equation, the first term refers to the energy of hydrophilic heads that are pulled apart to form the pore and the second term refers to the change in the interfacial energy. As pointed out above, some phospholipid heads protrude into the inner lining of the pore to partly neutralize the charge of peptides. There are several layers of phospholipid heads. In each layer (a horizontal plane of the pore), several phospoholipid heads lie along the circumference of the pore. Because of the repulsion between phospholipid heads, the center to center distance between two phospholipid heads is greater than its diameter d_h. Let this distance be $\left(1+\frac{1}{\kappa d_h}\right)d_h$, κ being Debye Huckel parameter. Since the phospholipids are bent along a circumference $(l+d_h)$, l and d_h being the length of the lipid tail and the diameter of the phospholipid head respectively, the number of layers n_{layers} of phospholipids in a pore is given by

$$n_{layers} = \frac{\pi(l+d_h)}{\left(1+\frac{1}{\kappa d_h}\right)d_h}.$$

The diameter of a pore d_{pore} consisting of n_a peptides and $n_a n_b$ phospholipids is therefore given by

$$d_{pore}(n_a, n_b) = \left(\frac{d_{pep} + \left(\frac{n_b}{n_{layers}}\right)d_h}{\pi}\right)n_a \quad (2)$$

The variation of $d_{pore}(n_a, n_b)$ with n_a for different values of n_b is given in Fig. S8 of supplemental information.

4.2. Free energy of peptide in aggregate

In addition, one should also include the free energy of peptide aggregate. When peptide molecules are moved from the bulk solution to the pore, the hydrophobic (outer) parts of the peptide are transferred from aqueous to hydrophobic environment. From the amino acid sequence of melittin, one can identify the hydrophobic side chains as Ile Ala Val Leu Val Leu Thr Thr Leu Pro Ala Leu Ile Ile. Therefore, from the knowledge of transfer free energies of these amino acid residues [26], one can calculate the hydrophobic free energy change Δg_{hy} as 1.085×10^5 J/mol. Because the peptide belonging to an aggregate within the pore is restricted in its movement (both translational and rotational), its entropy is decreased thus leading to an increase in its free energy. This increase is independent of pore size since it does not depend on peptide interactions with its neighbors. Let ξkT be the increase in free energy per peptide. The value of the parameter ξ will depend on the stiffness of peptide inside the pore. Consequently, the free energy change g_{en} is given by

$$g_{en}(n_a) = n_a\xi kT - n_a\Delta g_{hy} \quad (3)$$

4.3. Electrostatic free energy

The confinement of charge within the inner aqueous core of the pore will lead to electrostatic interactions of electrical double layers bounded by curved cylindrical surface. The Poisson Boltzmann equation inside the cylindrical cavity with constant surface charge density σ^* on the inner surface is given by

$$\frac{d^2\phi}{dX^2} + \frac{1}{X}\frac{d\phi}{dX} = \phi \quad (4)$$

where $X=\kappa r$, κ being Debye Huckel parameter, with the following boundary conditions:

$$X = 0, \quad \phi \text{ is finite}$$
$$X = \frac{\kappa d_{pore}}{2}, \quad \frac{d\phi}{dX} = \frac{\sigma^*}{\varepsilon_r\varepsilon_0\kappa} \quad (5)$$

whose solution is given by

$$\phi(X) = \frac{\sigma^*}{\varepsilon_r\varepsilon_0\kappa}\frac{I_0(X)}{I_1\left(\frac{\kappa d_{pore}}{2}\right)} \quad (6)$$

In the above equations, κ is the Debye Huckel parameter and the surface charge density

$$\sigma^* = \frac{(n_a q + n_a n_b q_{ph})e}{\pi d_{pore} t_{pore}} \tag{7}$$

and I_0 and I_1 are modified Bessel functions of the first kind. In the above equation, q_{ph} refers to the net charge of phospholipid head. The excess force per unit area f acting on the inner surface of the pore is given by [27]

$$f = kT\sum_i n_i^0 \left\{\exp\left(-\frac{z_i e\phi_0}{kT}\right) - 1\right\} + \varepsilon_r\varepsilon_0 \int_0^{d_{pore}/2} \frac{1}{r}\left(\frac{d\phi}{dr}\right)^2 dr \tag{8}$$

In the above equation, the first term on the right hand side is the osmotic pressure contribution because of the excess of counter ions as a result of overlap of double layers and the second term is due to curvature of the charged surface. It is to be noted that the second term is absent in case of planar double layers. Substituting the solution (6) in (8), we get

$$f(d_{pore}) = \frac{\sigma^{*2}}{\varepsilon_r\varepsilon_0 I_1^2\left(\frac{\kappa d_{pore}}{2}\right)}\left[\int_0^{\kappa d_{pore}/2} \frac{I_1^2(x)}{x}dx + \frac{1}{2}\right] = \frac{q_{net}^2 e^2}{\pi^2 d_{pore}^2 t_{pore}^2 \varepsilon_r\varepsilon_0 I_1^2\left(\frac{\kappa d_{pore}}{2}\right)}\left[\int_0^{\kappa d_{pore}/2} \frac{I_1^2(x)}{x}dx + \frac{1}{2}\right] \tag{9}$$

Therefore, the force experienced by a pore of diameter x with the same charge q_{net} is given by

$$F(x) = \frac{q_{net}^2 e^2}{\pi x t_{pore}\varepsilon_r\varepsilon_0 I_1^2\left(\frac{\kappa x}{2}\right)}\left[\int_0^{\kappa x/2} \frac{I_1^2(y)}{y}dy + \frac{1}{2}\right] \tag{10}$$

The potential energy g_e of charging the inner surface of a pore of diameter d_{pore} is therefore given by

$$g_e(n_a, n_b) = \int_{d_{pore}(n_a,n_b)}^{\infty} F(x)dx = \int_{d_{pore}(n_a,n_b)}^{\infty} \frac{q_{net}^2 e^2 \pi}{\pi x t_{pore}\varepsilon_r\varepsilon_0 I_1^2\left(\frac{\kappa x}{2}\right)}\left[\int_0^{\kappa x/2} \frac{I_1^2(y)}{y}dy + \frac{1}{2}\right]dx \tag{11}$$

Writing the above equation in terms of dimensionless variable, one obtains,

$$g_e(n_a, n_b) = \frac{q_{net}^2 e^2}{\pi t_{pore}} \int_{\kappa d_{pore}(n_a,n_b)}^{\infty} \frac{1}{\varepsilon_r\varepsilon_0 x I_1^2\left(\frac{x}{2}\right)}\left[\int_0^{x/2} \frac{I_1^2(y)}{y}dy + \frac{1}{2}\right]dx \tag{12}$$

4.4. Bending free energy

The phospholipid heads that line the pore are bent. Therefore, there is an increase in free energy as a result of bending of phospholipid head. Since the stretching modulus is much higher than the bending modulus, the area occupied by the phospholipid head in the inner lining of the pore can be assumed to be the same as that in the bilayer. The two principal radii of curvature for the bending of phospholipid head are $d_{pore}/2$, the radius of the pore and $t_{pore}/2$, the radius of the arc along which they are bent. Therefore, the bending energy is given by

$$g_{bend} = \frac{1}{2}K_c\left(\frac{2}{t_{pore}} + \frac{2}{d_{pore}}\right)^2 n_a n_b a_h \tag{13}$$

where K_c is the bending modulus of the bilayer.

Therefore, the change in free energy of pore ΔG_{sol} is given by

$$\Delta G_{sol}(n_a, n_b) = G_{pore}(n_a, n_b) - n_a G_{pep,sol} = g_{formation}(n_a, n_b) + g_e(n_a, n_b) + g_{bend}(n_a, n_b) + g_{en}(n_a) \tag{14}$$

Therefore, the free energy of pore with respect to adsorbed peptide on phospholipid bilayer is given by

$$\Delta G(n_a, n_b) = G_{pore}(n_a, n_b) - n_a G_{pep,ads} = \Delta G_{sol}(n_a, n_b) - n_a(G_{pep,ads} - G_{pep,sol}) \tag{15}$$

The difference in free energy between adsorbed melittin on phospholipid surface and melittin in solution can be obtained from the binding isotherm data for POPG as reported by Kuchinka and Seelig [22] via

$$\frac{(G_{pep,ads} - G_{pep,sol})}{kT} = \ln\left(\frac{1}{X}\right) \tag{16}$$

where X is moles of melittin that binds to a mole of phospholipid. The value of X depends on bulk melittin concentration. The experimental data of Kuchinka and Seelig gives a linear fit $X = K_b c$ with respect to the bulk melittin concentration c, K_b being the binding constant. The above equation can be recast as the sum of surface and bulk terms as

$$\Delta G(n_a, n_b) = \sigma_s \pi d_{pore}(n_a, n_b) - \frac{\pi}{4} d_{pore}(n_a, n_b)^2 \gamma \tag{17}$$

where σ_s is the surface free energy change per unit length for pore formation which is given by

$$\sigma_s = \frac{\lambda n_a d_{pep} + g_e(n_a, n_b) + g_{bend}(n_a, n_b) + g_{en}(n_a) - n_a(G_{pep,ads} - G_{pep,sol})}{\pi d_{pore}(n_a, n_b)} \tag{18}$$

At critical peptide concentration (analogous to solubility), pore formation is initiated with the critical pore size that is very large. Consequently, the surface free energy change per unit area at peptide concentrations above the critical concentration can be written as

$$\sigma = \sigma_s - \frac{kT\ln s}{\left(\frac{\pi d_{pore}(n_a,n_b)}{n_a}\right)} \tag{19}$$

where k is the Boltzmann constant, T is the temperature, $s = c_p/c_{ps}$ is supersaturation of peptide, c_p and c_{ps} being the peptide concentration and critical peptide concentration respectively. The denominator in the second term refers to the circumference of the pore per peptide. There is a critical pore radius at which the free energy of pore exhibits a maximum ΔG_{max} given by

$$\Delta G_{max} = \frac{\pi\sigma^2}{\gamma} \tag{20}$$

Peptides are added to existing pores by adsorption of peptides onto the liposome surface followed by surface diffusion. Pores also lose peptides as a result of their escape from the potential well arising from their interaction with their neighbors due to thermal motion. For pores of radius less than the critical radius, the rate of formation of pores is less than their rate of dissociation so that the pores are unstable [28]. On the other hand, pores of size greater than the critical pore size grow spontaneously since their rate of formation is greater than the rate of dissociation. The rate of nucleation of pores can be expressed as the flux

around the critical pore. Applying classical nucleation theory, one obtains the following expression for the rate of nucleation J of pores [28],

$$J = D_s \rho_{eq}(n_c)\sqrt{-\frac{\Delta G''(n_c)}{2\pi kT}} \tag{21}$$

where D_s is the surface diffusion coefficient of adsorbed peptide on bilayer surface, $\rho_{eq}(n_c)$ is the equilibrium surface concentration of pores of critical pore size and $\Delta G''(n_c)$ is the second derivative of variation of free energy of pore with number of peptides in the pore at the critical pore size. The equilibrium surface concentration of pores of critical size $\rho_{eq}(n_c)$ can be related to bulk peptide concentration c_p via [28]

$$\rho_{eq}(n_c) = \rho_{eq}(1)\exp\left(-\frac{\Delta G^*(n_c)}{kT}\right) = Kc_p \exp\left(-\frac{\Delta G^*(n_c)}{kT}\right) \tag{22}$$

where K is the equilibrium constant for adsorption of peptides onto liposome surface. In the above equation, $\rho_{eq}(1)$ refers to the surface concentration of adsorbed peptide on phospholipid surface. The surface concentration can be related to binding constant X as discussed above and is given by

$$\rho_{eq}(1) \sim \frac{K_b c_p}{2a_{lip}} \tag{23}$$

where K_b is the binding constant for melittin onto lipid and a_{lip} is the area of phospholipid head. Consequently, the equilibrium constant K in Eq. (22) is given by

$$K = \frac{K_b}{2a_{lip}} \tag{24}$$

Combining Eqs. (17)–(22), one obtains,

$$J = D_s K c_{ps} s\sqrt{-\frac{\Delta G''(n_c)}{2\pi kT}}\exp\left(-\frac{\pi\sigma_s^2}{\gamma kT}\left\{1 - \frac{n_a kT \ln s}{\pi\sigma_s d_{pore}(n_a, n_b)}\right\}^2\right) \tag{25}$$

Since $\ln s \ll 1$ for small supersaturations, we can retain only linear terms in the above equation to yield

$$J = D_s K c_{ps}\sqrt{-\frac{\Delta G''(n_c)}{2\pi kT}}\exp\left[-\frac{\pi\sigma_s^2}{\gamma kT}\right] s^{\frac{2n_a\sigma_s}{\gamma d_{pore}(n_a,n_b)}+1} \tag{26}$$

Since $-\Delta G'' = (\pi/2)\gamma(dd_{pore}/dn_a)$, using Eq. (2), the above equation can be recast as,

$$J = D_s K c_{ps}\frac{1}{2}\sqrt{\frac{\alpha\gamma}{kT}}\exp\left[-\frac{\pi\sigma_s^2}{\gamma kT}\right] s^{\frac{2n_a\sigma_s}{\gamma d_{pore}\left(n_a,n_b\right)}+1} \tag{27}$$

where $\alpha = d_{pep} + ((n_b/n_{layers})d_h)$. In order for the dye to leak through the pores, the pore size should be equal to or greater than the size of the dye molecule. Let n_{diff} be the minimum pore size for the dye to leak out. Pores of critical pore size n_c that are formed by nucleation have to grow to size n_{diff} before dye leakage. The growth of pore occurs by addition of peptide onto an existing pore by surface diffusion. The rate of peptide addition, therefore, can be expected to be proportional to peptide surface concentration $\rho_{eq}(1)$ on liposome surface. From Eq. (27), one can see that the rate of peptide addition to the pore is proportional to bulk peptide concentration c_p. If the peptide addition to a pore is assumed to be weakly dependent on pore size, the rate of growth $\dot{n}$ can be approximated as

$$\dot{n} = 2\pi D_s \frac{K_b}{2a_{lip}}\exp\left(-\frac{qe\zeta}{kT}\right) c_{ps} s \tag{28}$$

In the above equation, the exponential term is the electrostatic energy barrier for surface diffusion of melittin since the surface hopping of the molecule would require disengagement of electrostatic attraction between the charged sidechains and phospholipid head to move to neighboring phospholipid head. q is the net charge of melittin, e is the elementary charge and ζ is the zeta potential of liposomes. Therefore, the time of growth t_g of pore from size n_c to n_{diff} is given by

$$t_g = \frac{(n_{diff} - n_c)}{\dot{n}} \tag{29}$$

Denoting by $t = t' - t_{crit}$, where t' and t_{crit} refer to time and time of formation of critical pore size respectively, the pore size distribution is given by,

$$\begin{aligned} N(n,t) &= 0 \quad \text{if} \quad n < n_c \\ &= J\frac{(n - n_c)}{\dot{n}} \quad \text{if} \quad n_c < n < (n_c + \dot{n}t) \\ &= 0 \quad \text{if} \quad n > (n_c + \dot{n}t) \end{aligned} \tag{30}$$

where $N(n,t)$ is the number of pores of size n at time t. Therefore,

$$\begin{aligned} N(n_{diff},t) &= 0 \quad \text{if} \quad t < t_g \\ &= J(t - t_g) \quad \text{otherwise} \end{aligned} \tag{31}$$

Assuming quasi steady state diffusion of the dye from liposome to the surrounding aqueous medium through the pores, a mass balance for the dye gives,

$$\frac{dc_b}{dt} = \frac{6\phi}{\pi d_{lip}^3}\frac{D}{t_{pore}}\pi(c - c_b)\int_{n_{diff}}^{n_{\max}(t)} f(n)\left\{r(n)\right\}^2 dn \tag{32}$$

In the above equation, $f(n)dn$ is the number of pores of size n, $n + dn$, ϕ is the volume fraction of liposomes of diameter d_{lip}, D is the diffusion coefficient of the dye, c and c_b refer to the concentration of the dye inside the liposome and in the bulk respectively and $n_{\max}(t)$ is the maximum pore size at t. At time t, pore of size n and $n + dn$ are nucleated at times $t - t_g$ and $t - t_g - (dn/\dot{n})$ respectively. Therefore, the number of pores of critical pore size n_c that were formed between $t - t_g$ and $t - t_g - (dn/\dot{n})$ is $J(dn/\dot{n})$, As a result,

$$f(n) = \frac{J}{\dot{n}} \quad n > n_c \quad \text{and} \quad n_{\max}(t) = n_c + \dot{n}t \tag{33}$$

Substituting Eq. (33) in Eq. (32), one obtains,

$$\begin{aligned} \frac{dc_b}{dt} &= \frac{\phi}{2\pi d_{lip}^3}\frac{D}{t_{pore}}(c - c_b)\left[(n_c + \dot{n}t)^3 - (n_c + \dot{n}t_g)^3\right] D_s K c_{ps}\frac{1}{2\dot{n}} \\ &\quad \times\sqrt{\frac{\alpha\gamma}{kT}}\exp\left[-\frac{\pi\sigma_s^2}{\gamma kT}\right] s^{\frac{2n_a\sigma_s}{\gamma d_{pore}(n_a,n_b)}+1} \end{aligned} \tag{34}$$

Defining $\tau = n_c/\dot{n}$, Eq. (34) can be integrated to give the following equation for the evolution of dye concentration in the aqueous phase,

$$\ln\left(1 - \frac{c_b}{c}\right) = -\frac{\phi}{4\pi d_{lip}^3}\frac{D}{t_{pore}} D_s K c_{ps}\frac{1}{\dot{n}^2}\sqrt{\frac{\alpha\gamma}{kT}}\exp\left[-\frac{\pi\sigma_s^2}{\gamma kT}\right] s^{\frac{2n_a\sigma_s}{\gamma d_{pore}(n_a,n_b)}+1} n_c^4\left[\frac{1}{4}\left(1 + \frac{t}{\tau}\right)^4 - \left(1 + \frac{t_g}{\tau}\right)^3\left(1 + \frac{t}{\tau}\right) + \frac{3}{4}\left(1 + \frac{t_g}{\tau}\right)^4\right] \tag{35}$$

For small times, $t/\tau \ll 1$. Expanding the above equation by Taylor series and retaining terms only up to second order in t/τ, one obtains,

$$\ln\left(1-\frac{c_b}{c}\right) = -\frac{\phi}{4\pi d_{lip}^3}\frac{D}{t_{pore}}D_s K c_{ps}\frac{1}{\dot{n}^2}\sqrt{\frac{\alpha\gamma}{kT}}\exp\left[-\frac{\pi\sigma_s^2}{\gamma kT}\right] s^{\frac{2n_a\sigma_s}{\gamma d_{pore}(n_a,n_b)}+1} n_c^4\left[\frac{3}{2}\left(\frac{t^*}{\tau}\right)^2 - \frac{3}{2}\left(\frac{t_g}{\tau}\right)^2\right] \quad (36)$$

where $t^* = t' - t_{lag} = t - t_g$ since $t_{lag} = t_{crit} + t_g$. If the critical pore size is comparable to the size of fluorescent molecule, t_g/τ is small. For such a case,

$$\ln\left(1-\frac{c_b}{c}\right) \simeq -\frac{\phi}{4\pi d_{lip}^3}\frac{D}{t_{pore}}D_s K c_{ps}\frac{1}{\dot{n}^2}\sqrt{\frac{\alpha\gamma}{kT}} \times \exp\left[-\frac{\pi\sigma_s^2}{\gamma kT}\right] s^{\frac{2n_a\sigma_s}{\gamma d_{pore}(n_a,n_b)}+1} n_c^4\frac{3}{2}\left(\frac{t^*}{\tau}\right)^2 \quad (37)$$

Since $c_b/c = F/F_{max}$, Eq. (37) gives,

$$-\ln\left(1-\frac{F}{F_{max}}\right) \simeq \frac{\phi}{4\pi d_{lip}^3}\frac{D}{t_{pore}}D_s K\frac{1}{K_a^2 c_{ps}}\sqrt{\frac{\alpha\gamma}{kT}} \times \exp\left[-\frac{\pi\sigma_s^2}{\gamma kT}\right] s^{\frac{2n_a\sigma_s}{\gamma d_{pore}(n_a,n_b)}-1} n_c^4\frac{3}{2}\left(\frac{t^*}{\tau}\right)^2 \quad (38)$$

Plot of lag time t_{lag} vs melittin lipid ratio for three different dyes is shown in Fig. 2. The lag time is found to be in the order of FD20 > FD4 > calcein. Since the size of the three dye molecules increase in the order of calcein < FD4 < FD20, the time of growth t_g from critical pore size to the size of the dye molecule increases in the order of calcein < FD4 < FD20. Therefore, one would expect the lag time to increase in the order calcein < FD4 < FD20 since $t_{lag} = t_{crit} + t_g$. From Eq. (29), one obtains,

$$\frac{t_{lag,\mathrm{FD20}} - t_{lag,calcein}}{t_{lag,\mathrm{FD4}} - t_{lag,calcein}} = \frac{t_{g,\mathrm{FD20}} - t_{g,calcein}}{t_{g,\mathrm{FD4}} - t_{g,calcein}} = \frac{d_{\mathrm{FD20}} - d_{calcein}}{d_{\mathrm{FD4}} - d_{calcein}} \quad (39)$$

The size of FD4 and FD20 molecules are 14 and 33 nm respectively (Sigma product information). Since $d_{calcein}/d_{\mathrm{FD4}} = (MW_{calcein}/MW_{\mathrm{FD4}})^{1/3} = (622/4000)^{1/3}$, $d_{calcein} = 7.53$ nm. The experimental values of this ratio of differences in lag time (as defined by Eq. (39)) increases linearly with supersaturations from a value of around 1.7 at supersaturation of 1.1 to a value of 4.5 at supersaturation of 6. The predicted value of this ratio is 4.0. The experimental value agrees with the predicted value at supersaturation of five and higher. However, the experimental values of this ratio are found to be lower at lower supersaturations possibly as a result of higher experimental values of lag times for calcein due to experimental error. Initial slopes for the plots of $-\ln(1-F/F_{max})$ vs t^2 were determined for different supersaturations. The plot of $\ln(slope)$ vs $\ln s$ are shown in Fig. 5 for all the three dyes. The fitted values of the slopes of these plots are 3.16 for calcein, 0.3963 for FD4 and 0.4116 for FD20 respectively. If $t_g \ll \tau$, as per Eq. (34), this plot should give a slope of $\frac{2n_a\sigma_s}{\gamma d_{pore}(n_a,n_b)} - 1$. The length of hydrocarbon tail l and melittin diameter are taken as 4 and 1.12 nm respectively. The area of phospholipid head is taken as 0.965 nm^2 [29]. For melittin, the hydrophobic side chains are *Ile Ala Val Leu Val Leu Thr Thr Leu Pro Ala Leu Ile Ile*. Based on their transfer free energies [26], g_{hy} is estimated to be 1.085×10^5 J/mol. The energy barrier is higher for larger ξ (stiffer peptide in pore) and smaller n_b (smaller number of phospholipids in pore) as can be seen from the variation of free energy of pore with n_a for different values of n_b for fixed value of ξ as well as different values of ξ for fixed value of n_b given in Figs. S9a and S9b respectively. The calculated value of the slope from the analysis for different values of the parameters ξ and n_b are given in Table 1. The slope predicted by the model is found to be higher for larger values of the parameter ξ and smaller values of n_b. Under these conditions, the peptide assumes a much stiffer conformation within the pore and the pore has a larger confined charge (because of smaller number of phospholipid heads to neutralize the peptide charge) thus leading to higher energy barrier for nucleation. For largest n_b value, the calculated slope varies from 4.63 to 5.358 for different values of ξ. These values compare favorably with the values of 3.16 for calcein. This seems to indicate toroidal mechanism for pore formation with participation of large number of phospholipid heads. However, the slopes for FD4 and FD20 are found to be much smaller. This discrepancy is believed to be because the simplifying assumption of $t_g \ll \tau$ employed in the model is not valid in these cases since the size of the dye molecules are much larger than the critical pore size. In addition, the calculated values of nucleation rate of pores using Eqs. (21) and (22) are given in Table 1 which indicate that the rate of nucleation is found to be higher at larger values of n_b with a corresponding lower values of energy barrier for nucleation as a result of partial charge neutralization. At sufficiently higher values of n_b, however, the energy barrier is found to increase as a result of

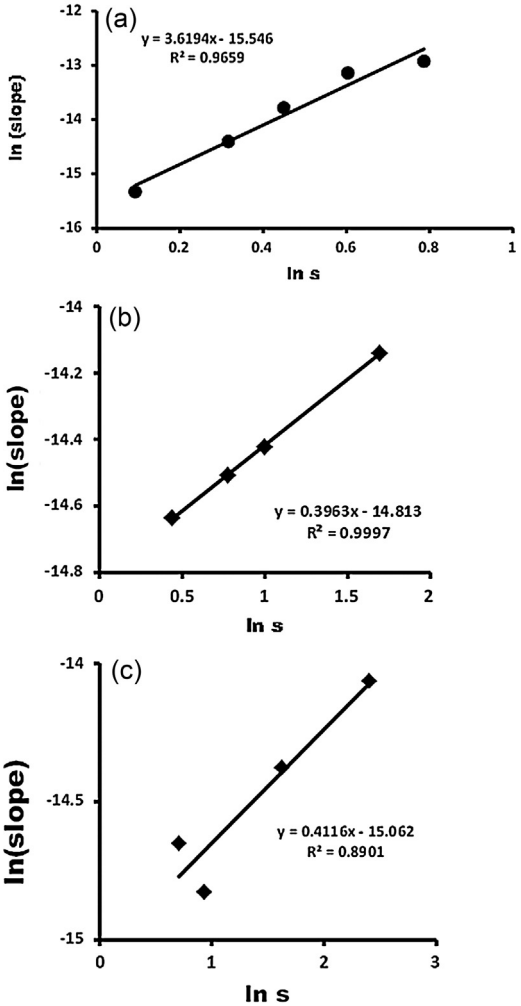

Fig. 5. Plot of $\ln(\mathrm{slope})$ of $-\ln(1-F/F_{max})$ vs t^2 plotted against $\ln s$ (a) calcein (b) FD4 and (c) FD20. The linear fit of the data is shown in the figures.

Table 1
Predicted values of the initial slope for the plots of $-\ln\left(1-F/F_{max}\right)$ vs t^2 as predicted by Eq. (35).

ξ	n_b	Slope	n^*	$\Delta G^*/kT$	log(J)
80	20	22.391	68	2810	−1222
	30	14.09	53	2474	−1076
	40	10.26	59	3046	−1324
	60	6.109	41	2637	−1146
	70	5.358	45	3120	−1356
70	20	19.98	58	2183	−949
	30	12.9	46	1979	−861
	40	9.55	52	2489	−1082
	60	6.17	36	2252	−979
	70	4.99	40	2693	−1170
60	20	18.45	48	1653	−718.92
	30	13.02	39	1557	−677.50
	40	11.36	44	2007	−872.93
	60	5.7	32	1907	−829.51
	70	4.63	36	2309	−1004
50	20	15.91	38	1215	−528.86
	30	10.98	52	1380	−600.51
	40	9.24	37	1211	−693.8

n^* is the value of n_a corresponding to critical pore size, $\Delta G^*/kT$ is the dimensionless energy barrier and J is the rate of nucleation of critical pores. The parameter values employed in these calculations are: $\Delta g_{hy} = 1.085 \times 10^5$ J/mol [26], $\sigma = 6.5 \times 10^{-3}$ N/m, $\lambda = 3.9 \times 10^{-11}$ J/m, $d_{pep} = 1.12 \times 10^{-9}$ m, $t_{pore} = 5 \times 10^{-9}$ m, $I = 0.1$, $q = 5$, $K_{bend} = 4.1 \times 10^{-19}$ J [30], $d_h = 3.86 \times 10^{-10}$m, $q_h = -0.059$, $T = 298$ K, $D_s = 4 \times 10^{-15}$ m^2 s^{-1} [31], $K_b = 0.0013$ (μM)$^{-1}$ [22].

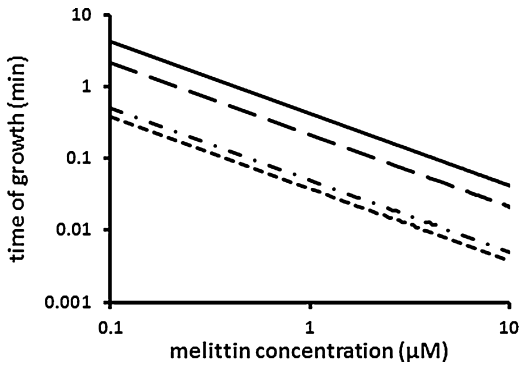

Fig. 6. Plot of time of growth of critical pore to size of FD20 dye as a function of melittin concentration. The time of growth t_g as calculated using Eq. (29) is the time for the critical pore to grow to a size of 33 nm. Solid line refers to $\xi = 50$; $n_b = 20$; Dashed line refers to $\xi = 50$; $n_b = 40$; double broken line refers to $\xi = 60$; $n_b = 60$; small broken line refers to $\xi = 60$ $n_b = 40$.

predominant contribution of bending free energy of phospholipid heads thereby resulting in a lower rates of nucleation. The time of growth of critical pore to a size of FD 20 molecule (33 nm) was calculated using Eq. (29) for different bulk melittin concentration for different values of flexibility parameter ξ and number of phospholipids per melittin in a pore n_b. These results are shown in Fig. 6. The time of growth is found to decrease with an increase in melittin concentration and is inversely proportional to concentration. The time of growth t_g is found to be smaller at higher flexibility parameter ξ and larger values of n_b (Fig. 6).

5. Conclusions

Evolution of fluorescence intensity due to leakage of dyes of different sizes from liposome by melittin of different concentrations indicated a critical melittin concentration for pore formation and a lag time above this critical concentration which was larger for lower melittin concentration as well as for larger size of dye molecule. The rate of dye leakage following the lag time was found to be larger at higher melittin concentration. A mathematical model for nucleation and growth of pores formed by an aggregate of melittin in lipid bilayer is proposed. The difference in the lag time for dye leakage for the three dyes of different sizes is shown to be due to the difference in the time of growth of pores from the critical pore size to the size of the molecule. Model prediction of variation of dye leakage rate with melittin concentration agreed fairly well with the experimental data for calcein and seems to suggest a toroidal mechanism of pore formation with participation of large number of phospholipid heads.

Acknowledgements

We would like to acknowledge the financial support provided to L.Z. by the Chinese government and by the Whistler Center for Carbohydrate Research, Purdue University.

Appendix A. Supplementary data

Supplementary material related to this article can be found, in the online version, at http://dx.doi.org/10.1016/j.colsurfb.2014.09.037.

References

[1] R. Gennaro, M. Zanetti, Structural features and biological activities of the cathelicidin-derived antimicrobial peptides, Biopolymers 55 (1) (2000) 31–49.
[2] R.E.W. Hancock, H.G. Sahl, Antimicrobial and host-defense peptides as new anti-infective therapeutic strategies, Nat. Biotechnol. 24 (12) (2006) 1551–1557.
[3] K.A. Brogden, Antimicrobial peptides: pore formers or metabolic inhibitors in bacteria? Nat. Rev. Microbiol. 3 (3) (2005) 238–250.
[4] M.T. Lee, F.Y. Chen, H.W. Huang, Energetics of pore formation induced by membrane active peptides, Biochemistry 43 (12) (2004) 3590–3599.
[5] K. Matsuzaki, Magainins as paradigm for the mode of action of pore forming polypeptides, Biochim. Biophys. Acta 1376 (3) (1998) 391–400.
[6] K.J. Hallock, D.K. Lee, A. Ramamoorthy, MSI-78, an analogue of the magainin antimicrobial peptides, disrupts lipid bilayer structure via positive curvature strain, Biophys. J. 84 (5) (2003) 3052–3060.
[7] A.S. Ladokhin, M.E. Selsted, S.H. White, Sizing membrane pores in lipid vesicles by leakage of co-encapsulated markers: pore formation by melittin, Biophys. J. 72 (4) (1997) 1762–1766.
[8] B. Bechinger, The structure, dynamics and orientation of antimicrobial peptides in membranes by multidimensional solid-state NMR spectroscopy, Biochim. Biophys. Acta 1462 (1–2) (1999) 157–183.
[9] K.F. Wang, R. Nagarajan, T.A. Camesano, Antimicrobial peptide alamethicin insertion into lipid bilayer: a QCM-D exploration, Colloids Surf. B: Biointerfaces 116 (2014) 472–481.
[10] H.W. Huang, Action of antimicrobial peptides: two-state model, Biochemistry 39 (29) (2000) 8347–8352.
[11] F.Y. Chen, M.T. Lee, H.W. Huang, Evidence for membrane thinning effect as the mechanism for peptide-induced pore formation, Biophys. J. 84 (6) (2003) 3751–3758.
[12] L. Yang, et al., Barrel-stave model or toroidal model? a case study on melittin pores, Biophys. J. 81 (3) (2001) 1475–1485.
[13] K. Matsuzaki, et al., An antimicrobial peptide, magainin 2, induced rapid flip-flop of phospholipids coupled with pore formation and peptide translocation, Biochemistry 35 (35) (1996) 11361–11368.
[14] Y. Shai, Mechanism of the binding, insertion and destabilization of phospholipid bilayer membranes by alpha-helical antimicrobial and cell non-selective membrane-lytic peptides, Biochim. Biophys. Acta 1462 (1–2) (1999) 55–70.
[15] A.S. Ladokhin, S.H. White, 'Detergent-like' permeabilization of anionic lipid vesicles by melittin, Biochim. Biophys. Acta 1514 (2) (2001) 253–260.
[16] T. Nguyen, K.P. McNamara, Z. Rosenzweig, Optochemical sensing by immobilizing fluorophore-encapsulating liposomes in sol–gel thin films, Anal. Chim. Acta 400 (1999) 45–54.
[17] A.V. Popova, A.G. Heyer, D.K. Hincha, Differential destabilization of membranes by tryptophan and phenylalanine during freezing: the roles of lipid composition and membrane fusion, Biochim. Biophys. Acta 1561 (1) (2002) 109–118.
[18] S.C. Park, et al., A plausible mode of action of pseudin-2, an antimicrobial peptide from Pseudis paradoxa, Biochim. Biophys. Acta 1808 (1) (2011) 171–182.
[19] R.H. Bisby, C. Mead, C.G. Morgan, Active uptake of drugs into photosensitive liposomes and rapid release on UV photolysis, Photochem. Photobiol. 72 (1) (2000) 57–61.
[20] D. Needham, T.J. Mcintosh, E. Evans, Thermomechanical and transition properties of dimyristoylphosphatidylcholine cholesterol bilayers, Biochemistry 27 (13) (1988) 4668–4673.
[21] J.G. Lees, et al., A reference database for circular dichroism spectroscopy covering fold and secondary structure space, Bioinformatics 22 (16) (2006) 1955–1962.

[22] E. Kuchinka, J. Seelig, Interaction of melittin with phosphatidylcholine membranes – binding isotherm and lipid headgroup conformation, Biochemistry 28 (10) (1989) 4216–4221.
[23] F.Y. Chen, M.T. Lee, H.W. Huang, Sigmoidal concentration dependence of antimicrobial peptide activities: a case study on alamethicin, Biophys. J. 82 (2) (2002) 908–914.
[24] K. He, et al., Antimicrobial peptide pores in membranes detected by neutron inplane scattering, Biochemistry 34 (48) (1995) 15614–15618.
[25] K. He, et al., Neutron scattering in the plane of membranes: structure of alamethicin pores, Biophys. J. 70 (6) (1996) 2659–2666.
[26] C.R. Cantor, P.R. Schimmel, Biophysical Chemistry, Part I; The Conformation of Biological Macromolecules, W.H. Freeman and Company, New York, 1980.
[27] Y.H. Yang, J. Walz, P. Pintauro, Curvature effects on electric double-layer forces. 1. Comparisons with parallel-plate geometry, J. Chem. Soc.–Faraday Trans. 91 (17) (1995) 2827–2836.
[28] Kalikmanov, Nucleation Theory. Lecture Notes in Physics, vol. 860, Springer, 2013.
[29] L.J. Lis, et al., Interactions between neutral phospholipid bilayer membranes, Biophys. J. 37 (3) (1982) 657–665.
[30] H.P. Duwe, J. Kaes, E. Sackmann, Bending elastic moduli of lipid bilayers: modulation by solutes, J. Phys. France 51 (1990) 945–962.
[31] R.J. Cherry, Rotational and lateral diffusion of membrane-proteins, Biochim. Biophys. Acta 559 (4) (1979) 289–327.